A "v^2-f BASED" MACROSCOPIC k-ε MODEL FOR TURBULENT FLOW THROUGH POROUS MEDIA

S. Kazemzadeh Hannani* and R. Bahoosh Kazerooni

Center of Excellence in Energy Conversion, School of Mechanical Engineering
Sharif University of Technology, P.O. Box 11155-9567, Tehran, Iran
hannani@sina.sharif.ac.ir – bahoosh@mehr.sharif.edu

*Corresponding Author

(Received: March 3, 2008 - Accepted in Revised Form: May 8, 2008)

Abstract In this paper a new macroscopic k-ε model is developed and validated for turbulent flow through porous media for a wide range of porosities. The morphology of porous media is simulated by a periodic array of square cylinders. In the first step, calculations based on microscopic $\overline{v^2}-f$ model are conducted using a Galerkin/Least-Squares finite element formulation, employing equal order bilinear velocity-pressure elements. Calculations are validated by comparing the results to available data in the literature. In the second step, the volume averaged properties are extracted from the microscopic solution of $\overline{v^2}-f$ model. Then, employing the volume average technique, the macroscopic transport equations of continuity, momentum and k-ε model are derived and modeled. In the third step and during the volume averaging process, additional terms appeared in the k-ε model are interpreted and compared with the volume averaged properties that are extracted from the solution of microscopic $\overline{v^2}-f$ model. Finally a "$\overline{v^2}-f$ based" macroscopic k-ε model is developed and validated successfully for a wide range of porosities by comparing the macroscopic data to those predicted by microscopic $\overline{v^2}-f$ model. Moreover, the results of the calculations are compared with the result of an experimental work in the literature in order to validate the accuracy of the model.

Keywords Porous, Turbulence, k-ε, $\overline{v^2}-f$

چکیده در این مقاله، یک مدل جدید ماکروسکوپیک k-ε برای شبیه سازی جریان در محیط های متخلخل برای محدودهٔ وسیعی از ضرایب تخلخل توسعه داده شده و معتبر سازی شده است. هندسه و آرایش ذرات محیط متخلخل توسط یک ردیف استوانه با مقطع مربعی که بصورت تناوبی گسترش می یابد، مدل گردیده است. در گام اول، محاسبات با استفاده از مدل $\overline{v^2}-f$ و روش عددی اجزاء محدود (گالرکین حداقل مربعات) با بکارگیری المان های هم مرتبه برای فشار و سرعت از دیدگاه میکروسکوپی انجام شد و نتایج با جواب های سایر مطالعات مقایسه و معتبر سازی گردید. درگام دوم مقادیر متوسط حجمی از نتایج حل میکروسکوپیک محاسبه شد و با استفاده از تکنیک متوسط گیری حجمی معادلات پیوستگی، ممنتوم و معادلات مدل k-ε در حالت ماکروسکوپیک استخراج و سپس مدل سازی شدند. درگام سوم، جملات اضافی ناشی از متوسط گیری حجمی توسط نتایج حاصل از مدل $\overline{v^2}-f$ مدل سازی و سپس در محدودهٔ وسیعی از ضرایب تخلخل معتبر سازی شدند. همچنین شبیه سازی یک مسئله با جواب های تجربی موجود انجام شد و اعتبار قابل قبول مدل حاضر تائید گردید.

1. INTRODUCTION

Existence of turbulent flow or turbulence, in general, in porous media with considerable permeability are reported by many experimentalists. Based on the flow visualization techniques, turbulent flow through porous media occurs at $Re_p > 300$ [1]. Simulating flow through compact heat exchangers, composite break-waters or seawalls, casting of binary alloys with electromagnetic stirring and flow through the core of nuclear power plant, designing fluidized bed

combustors, and petroleum extraction are a few recent applications of turbulent flow through porous media [2-7].

A zero equation macroscopic turbulence model was derived by Masuoka, et al [8] and a one equation macroscopic turbulence model was proposed by Alvarez, et al [9] for flow through porous media. Antohe, et al [10] applied the time averaging operator to the generalized model (known as the Brinkman-Forchheimer-Extended Darcy model) and derived a two equation for macroscopic turbulence model. This work was extended by Getachew, et al [11] in order to take into account the Forchheimer term into a higher order.

Following another approach, Kuwahara, et al [12], Nakayama, et al [13], and Pedras, et al [14] conducted numerical experiments for turbulent flows through porous media by mimicking the porous media with using a periodic array of cylinders. They used the conventional 'microscopic' two-equation turbulence model based on RANS equations and derived a two equation macroscopic turbulence model by volume averaging technique in different ways. For more information on 'macroscopic' turbulence modeling see the recent book of de Lemos [15]. Kuwahara, et al [16] performed Large-eddy Simulation (LES) as a 'microscopic' point of view and compared k-ε models' data of [13] with the results of LES. Chandesris, et al [7] derived a macroscopic k-ε model adapted to longitudinal flows in channels, pipes and rod bundles which is suited for flow through the core of nuclear power.

Deriving the macroscopic transport equations for incompressible flow in porous media is based mathematically upon the volume-average methodology. Applying the volume average operator over the standard fluid transport equations in a representative elementary volume, REV, (see Section 3) will produce additional terms. Proposing a closure model for these additional terms in the volume averaged governing equations is the main difficulty of macroscopic turbulence modeling. In order to conserve as much information of the microscopic flow field, the size of REV should be sufficiently small as possible in the volume-averaged flow field. Macroscopic variables are defined as a suitable mean over an adequately large representative elementary volume.

During the last few years, the $\overline{v^2}-f$ (DNS based) turbulence model, originally introduced by Durbin, et al [17-19], has become increasingly popular due to its ability to correctly account for near-wall damping without the use of ad-hoc damping functions. Wall effects through porous media and strong blockage of the flow in stagnation and impingement region of pores are very crucial; therefore it seems that $\overline{v^2}-f$ model is a good candidate.

In this work, by applying the volume averaging technique, a macroscopic k-ε turbulence model has been derived. The additional terms that appear in the volume averaged process of k-ε model are interpreted and compared with the volume averaged properties that is extracted from the solution of microscopic $\overline{v^2}-f$ model. Finally a "$\overline{v^2}-f$ based" macroscopic k-ε model is developed. The governing equations are discretized using GLS (Galerkin/Least-Squares) finite element method employing equal order bilinear interpolation for velocity and pressure and other variables in conjunction with a pressure stabilizing method. This technique circumvents the stability condition and equal order velocity pressure elements can be employed.

2. MICRSCOPIC GOVERNING EQUATIONS AND $\overline{v^2}-f$ MODEL

For incompressible flow, the mean flow variables satisfy the following Reynolds Averaged Navier-Stokes equations (RANS):

$$\nabla \cdot U = 0 \tag{1}$$

$$\frac{DU}{Dt} = -\frac{1}{\rho}\nabla p + \nabla \cdot \left[\left(\nu + \nu_t \right) \left(\nabla U + \nabla U^{T} \right) \right] \tag{2}$$

The turbulent viscosity ν_t is obtained by the $\overline{v^2}-f$ model. This model is valid up to the wall and circumvents the use of wall functions (see below). The eddy viscosity ν_t is given by:

$$\nu_t = C_\mu \overline{v^2} T \tag{3}$$

The $\overline{v^2} - f$ model of Durbin [17-19] and Behnia, et al [20] comprises of solving two extra equations, the wall-normal stress $\overline{v^2}$ transport equation and an elliptic relaxation function f equation with respect to the standard k and ε model. The stress-strain relationship is Boussinesq approximation and given as:

$$\overline{u_i u_j} - \frac{2}{3}\delta_{ij} k = -\nu_t \left(\frac{\partial U_i}{\partial x_j} + \frac{\partial U_j}{\partial x_i} \right) \tag{4}$$

Lien, et al [21] generated a new variable for elliptic relaxation function (compensated $\tilde{f}$). This modification allows a simple explicit boundary condition at walls for elliptic relaxation and can be summarized by the following transport equations [21]:

$$\frac{\partial k}{\partial t} + U_j \frac{\partial k}{\partial x_j} = \frac{\partial}{\partial x_j}\left[\left(\nu + \frac{\nu_t}{\sigma_k} \right) \frac{\partial k}{\partial x_j} \right] + P_k - \varepsilon \tag{5}$$

$$\frac{\partial \varepsilon}{\partial t} + U_j \frac{\partial \varepsilon}{\partial x_j} = \frac{\partial}{\partial x_j}\left[\left(\nu + \frac{\nu_t}{\sigma_k} \right) \frac{\partial \varepsilon}{\partial x_j} \right] + \frac{C_{\varepsilon 1} P_k - C_{\varepsilon 2}}{T} \tag{6}$$

$$\frac{\partial \overline{v^2}}{\partial t} + U_j \frac{\partial \overline{v^2}}{\partial x_j} = \frac{\partial}{\partial x_j}\left[\left(\nu + \frac{\nu_t}{\sigma_k} \right) \frac{\partial \overline{v^2}}{\partial x_j} \right] - \overline{v^2} \frac{\varepsilon}{k} + k f \tag{7}$$

$$\tilde{f} - L^2 \nabla^2 \tilde{f} = \left[\frac{2}{3} C_1 + (5 - C_1) \frac{\overline{v^2}}{k} \right] \frac{1}{T} + C_2 \frac{P_k}{k} \tag{8}$$

P_k is the production of turbulent kinetic energy and is defined as:

$$P_k = \overline{u_i u_j} \partial U_i / \partial x_j \tag{9}$$

In Equations 6-8, T and L are time and length scale respectively and are given as [21]:

$$T = \text{Min}\left[\text{Max}\left[\frac{k}{\varepsilon}, C_T \sqrt{\frac{\nu}{\varepsilon}} \right], \frac{0.6k}{\sqrt{6} C_\mu \overline{v^2} S} \right] \tag{10}$$

$$L = C_L \text{Max}\left[\text{Min}\left[\frac{k^{3/2}}{\varepsilon}, \frac{k^{3/2}}{\sqrt{6} C_\mu \overline{v^2} S} \right], C_\eta \frac{\nu^{3/4}}{\varepsilon^{1/4}} \right] \tag{11}$$

The coefficients of the modified model are as follows [21]:

$$C_\mu = 0.22,\ C_L = 0.23,\ C_\eta = 85,\ C_T = 6.,\ C_1 = 0.4,\ C_2 = 0.3,\ C_{\varepsilon 2} = 1.9,\ \sigma_k = 1.,\ \sigma_\varepsilon = 1.3,\ C_{\varepsilon 1} = 1.4\left[1 + 0.045 \sqrt{\frac{k}{\overline{v^2}}} \right] \tag{12}$$

Mean strain rate tensor S_{ij} is given as:

$$S_{ij} = \left(\partial U_i / \partial x_j + \partial U_j / \partial x_i \right) / 2 \tag{13}$$

In Equations 10 and 11, S is the strain-rate magnitude and is defined as:

$$S = \sqrt{S_{ij} S_{ij}} \tag{14}$$

The no-slip boundary conditions for turbulent variables ($y \to 0$) are approximated as:

$$k_w = 0,\ \varepsilon_w = \lim_{y \to 0} \frac{2\nu k}{y^2},\ \overline{v_w^2} = 0,\ f_w = 0 \tag{15}$$

Variable y denotes the normal distance to the wall.

It is known that the $\overline{v^2} - f$ model has a poor

numerical stability. Sveningsson, et al [22] and Davidson, et al [23] proposed a simple restriction for improving the numerical stability. In this work, these restrictions are imposed.

3. THE VOLUME AVERAGE TECHNIQUE

The volumetric volume average of any scalar, spatially vector or second order tensor associated with the fluid-phase (B) over V is defined as follows:

$$\langle B\rangle^{v} = \frac{1}{V}\int_{V} B dV \tag{16}$$

Where the elementary volume is shown in Figure 1, and the intrinsic volume average is defined as:

$$\langle B\rangle^{f} = \frac{1}{V}\int_{V_f} B dV \tag{17}$$

The porosity of the porous medium is defined as:

$$\varphi = \frac{V_f}{V} \tag{18}$$

V_f is the volume occupied with fluid and V is the total volume.

The volumetric and intrinsic averaged are related to porosity φ as follows:

$$\langle B\rangle^{f} = \varphi \langle B\rangle^{v} \tag{19}$$

Relationships between the volume averaged of derivatives and the derivatives of the volume averaged properties are needed in the averaging process of transport governing equations. These relationships are derived in a number of works, (for more detail see Whitaker [24], Gray, et al [25]) and the total process is known as the theorem of local volumetric average [10]. The relationships are written as [10]:

$$\langle \nabla B\rangle^{f} = \nabla\left(\varphi\langle B\rangle^{f}\right) + \frac{1}{V}\int_{A_w} B n dA \tag{20}$$

$$\langle \nabla \cdot B\rangle^{f} = \nabla\cdot\left(\varphi\langle B\rangle^{f}\right) + \frac{1}{V}\int_{A_w} B\cdot n dA \tag{21}$$

$$\left\langle \frac{\partial B}{\partial t}\right\rangle^{f} = \frac{\partial}{\partial t}\left(\varphi\langle B\rangle^{f}\right) + \frac{1}{V}\int_{A_w} n\cdot(uB) dA \tag{22}$$

where A_w and u are the interfacial area and velocity of fluid-phase, n is the unit vector normal to A_w. The area A_w is not the area surrounding the volume ΔV in Figure 1.

Double prime is defined as deviation of the quantity B from the intrinsic volume average in this work:

$$B = \langle B\rangle^{f} + B'' \tag{23}$$

The macroscopic continuity and momentum equations through porous media can be obtained by volume averaging the corresponding microscopic equations over a REV, such as ΔV_f (Figure 1). Following [13] the macroscopic continuity and macroscopic momentum equation are written as follows:

$$\nabla\cdot\langle U\rangle^{f} = 0 \tag{24}$$

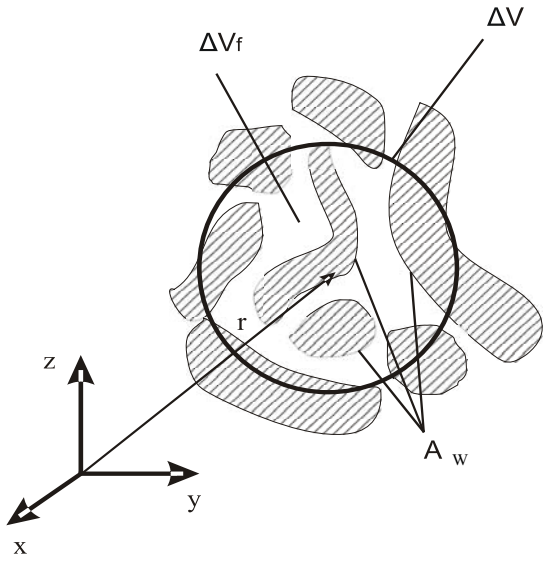

Figure 1. R. E. V, the representative elementary ume.

$$\frac{D\langle U\rangle^f}{Dt} = -\frac{1}{\rho}\nabla\langle p\rangle^f + \nabla\cdot\left[\left(\nu+\nu_t\right)\left(\nabla\langle U\rangle^f + \nabla\left\langle U^T\right\rangle^f\right)\right] - \left(\frac{\nu}{K}+\frac{\varphi F}{\sqrt{K}}\left(\langle U\rangle^f\cdot\langle U\rangle^f\right)^{\frac{1}{2}}\right)\langle U\rangle^f \quad (25)$$

These equations are derived by applying the volume averaging technique to Equations 1 and 2 (see [13] for details). The additional integrals which appear in the process of averaging the momentum equation are modeled with well known Darcy and Forchheimer terms (see [13,14] for details), where permeability K and Forchheimer constant F are approximated by Equations 26 and 27, respectively, (see [26] for details).

$$K = \frac{\varphi^3 d_p^2}{150(1-\varphi)^2} \quad (26)$$

$$F = \frac{1.75}{\sqrt{150\varphi^3}} \quad (27)$$

For deriving the macroscopic k-ε model we have to apply the volume average operator over k and ε transport equations of "clear flow" (microscopic or non-averaged) which is illustrated in the sequel.

4. TRANSPORT EQUATIONS FOR $\langle k\rangle^f$ AND $\langle\varepsilon\rangle^f$

Standard k and ε transport equations are employed to derive the macroscopic k-ε model:

$$\frac{\partial k}{\partial t} + U_j\frac{\partial k}{\partial x_j} = \frac{\partial}{\partial x_j}\left[\left(\nu+\frac{\nu_t}{\sigma_k}\right)\frac{\partial k}{\partial x_j}\right] + P_k - \varepsilon \quad (28)$$

$$\frac{\partial \varepsilon}{\partial t} + U_j\frac{\partial \varepsilon}{\partial x_j} = \frac{\partial}{\partial x_j}\left[\left(\nu+\frac{\nu_t}{\sigma_k}\right)\frac{\partial \varepsilon}{\partial x_j}\right] - \left(C_1P_k + C_2\varepsilon\right)\frac{\varepsilon}{k} \quad (29)$$

The turbulent viscosity and model constants are given as [27]:

$$\nu_t = C_D\frac{k}{\varepsilon^2} \quad (30)$$

$$C_\mu = 0.09,\ C_1 = 1.44,\ C_2 = 1.92,\ \sigma_k = 1.,\ \sigma_\varepsilon = 1.3 \quad (31)$$

Macroscopic turbulent viscosity is defined by macroscopic values $\langle k\rangle^f, \langle\varepsilon\rangle^f$, therefore it is assumed constant in the REV (V_f). Applying the volume average operator over Equation 4 leads to macroscopic eddy viscosity relationship:

$$-\left\langle\overline{u_iu_j}\right\rangle^f = 2\nu_t\left\langle S_{ij}\right\rangle^f - \frac{2}{3}\langle k\rangle^f\delta_{ij} \quad (32)$$

Using (21), $\left\langle S_{ij}\right\rangle^f$ can be expanded as follows:

$$\left\langle S_{ij}\right\rangle^f = \frac{1}{2}\left\langle\left(\frac{\partial U_i}{\partial x_j}+\frac{\partial U_j}{\partial x_i}\right)\right\rangle^f = \frac{1}{2}\left\{\frac{\partial}{\partial x_j}\left(\langle U_i\rangle^f\right) + \frac{\partial}{\partial x_i}\left(\langle U_j\rangle^f\right) + \frac{1}{\Delta V_f}\int_{A_w}\left[n_jU_i + n_iU_j\right]dA\right\} \quad (33)$$

Noting that at the interface area A_w, $U_i = 0$, therefore the integral term in (33) is neglected:

$$\left\langle S_{ij}\right\rangle^f = \frac{1}{2}\left\{\frac{\partial}{\partial x_j}\left(\langle U_i\rangle^f\right) + \frac{\partial}{\partial x_i}\left(\langle U_j\rangle^f\right)\right\} \quad (34)$$

Hence the macroscopic Reynolds stress is derived as:

$$-\left\langle\overline{u_iu_j}\right\rangle^f = \nu_t\left[\frac{\partial}{\partial x_j}\left(\langle U_i\rangle^f\right) + \frac{\partial}{\partial x_i}\left(\langle U_j\rangle^f\right)\right] - \frac{2}{3}\langle k\rangle^f\delta_{ij} \quad (35)$$

Implementing the intrinsic volume average

operator over the Equation 28 for each term and using relations (20) to (22) leads to:

$$\left\langle \frac{\partial k}{\partial t} \right\rangle^f = \frac{\partial}{\partial t}\left(\langle k \rangle^f \right) - \frac{1}{\Delta V_f} \int_{A_w} n_i \left(U_i k \right) dA \qquad (36)$$

$$\left\langle \frac{\partial}{\partial x_i}\left(U_i k \right) \right\rangle^f = \frac{\partial}{\partial x_i}\left(\langle U_i k \rangle^f \right) + \frac{1}{\Delta V_f} \int_{A_w} n_i \left(U_i k \right) dA \qquad (37)$$

At interface A_w we have $U = u = k = 0$, thus the integral terms in Equations 36 and 37 are vanished. On the right-hand side of Equation 37 the first term can be expanded as:

$$\frac{\partial}{\partial x_i}\left(\langle U_i k \rangle^f \right) = \frac{\partial}{\partial x_i}\left[\langle U_i \rangle^f \langle k \rangle^f + \langle U_i'' k'' \rangle^f \right] \qquad (38)$$

Following the arguments of [14], the first term on the right-hand side of Equation 38 is the convection of $\langle k \rangle^f$ related to the macroscopic velocity. Convective transport caused by spatial deviation of both k and U_i is presented by the second term.

Applying the volume average operator over the diffusion term of Equation 28 leads to:

$$\left\langle \frac{\partial}{\partial x_i}\left[\left(\nu + \frac{\nu_t}{\sigma_k} \right) \frac{\partial k}{\partial x_i} \right] \right\rangle^f = \frac{\partial}{\partial x_i}\left\{ \left\langle \left(\nu + \frac{\nu_t}{\sigma_k} \right) \frac{\partial k}{\partial x_i} \right\rangle^f \right\} +$$
$$\frac{1}{\Delta V_f} \int_{A_w} n_i \left[\left(\nu + \frac{\nu_t}{\sigma_k} \right) \frac{\partial k}{\partial x_i} \right] dA \quad \Rightarrow$$
$$= \frac{\partial}{\partial x_i}\left[\left(\nu + \frac{\nu_t}{\sigma_k} \right) \frac{\partial \langle k \rangle^f}{\partial x_i} + \frac{1}{\Delta V_f} \int_{A_w} n_i k dA \right] +$$
$$\frac{1}{\Delta V_f} \int_{A_w} n_i \left[\left(\nu + \frac{\nu_t}{\sigma_k} \right) \frac{\partial k}{\partial x_i} \right] dA \qquad (39)$$

Following [14], we can expand $\nabla \cdot \nabla k$ as bellow:

$$\nabla \cdot \nabla k = \frac{1}{2} \nabla \cdot \nabla \left(\overline{u \cdot u} \right) = \nabla \cdot \overline{\left[u \cdot \left(\nabla u \right)^T \right]} \qquad (40)$$

By using Equation 40, Equation 39 can be rewritten as:

$$\left\langle \frac{\partial}{\partial x_i}\left[\left(\nu + \frac{\nu_t}{\sigma_k} \right) \frac{\partial k}{\partial x_i} \right] \right\rangle^f = \frac{\partial}{\partial x_i}\left[\left(\nu + \frac{\nu_t}{\sigma_k} \right) \frac{\partial \langle k \rangle^f}{\partial x_i} \right] +$$
$$\frac{\partial}{\partial x_i}\left(\frac{1}{\Delta V_f} \int_{A_w} n_i k dA \right) + \frac{1}{\Delta V_f} \int_{A_w} n_j u_i \frac{\partial u_j}{\partial x_i} dA \qquad (41)$$

Therefore the integral terms in the right-hand side of Equation 41 are disappeared because at interface A_w, k and u_i are vanished.

Production term of transport equation of k can be averaged as below:

$$\left\langle 2\nu_t S_{ij} S_{ij} \right\rangle^f = 2\nu_t \left\langle S_{ij} \right\rangle^f \left\langle S_{ij} \right\rangle^f + R^k_{Product} \qquad (42)$$

All of remainders of averaging process of production term is denoted as $R^k_{Product}$. Volume averaged of last term is $\langle \varepsilon \rangle^f$ obviously.

After the averaging process, transport equation of $\langle k \rangle^f$ becomes:

$$\frac{\partial \langle k \rangle^f}{\partial t} + \frac{\partial}{\partial x_i}\left(\langle U_i \rangle^f \langle k \rangle^f \right) = \frac{\partial}{\partial x_i}\left[\left(\nu + \frac{\nu_t}{\sigma_k} \right) \frac{\partial \langle k \rangle^f}{\partial x_i} \right] +$$
$$2\nu_t \left\langle S_{ij} \right\rangle^f \left\langle S_{ij} \right\rangle^f - \langle \varepsilon \rangle^f - \frac{\partial}{\partial x_i}\left[\langle U_i'' k'' \rangle^f \right] +$$
$$\frac{1}{\Delta V_f} \int_{A_w} n_i \left[\left(\nu + \frac{\nu_t}{\sigma_k} \right) \frac{\partial k}{\partial x_i} \right] dA + R^k_{Product} \qquad (43)$$

Note that, all spatial and time derivatives in steady state fully developed flow through homogenous porous media become negligible, therefore $\langle \varepsilon \rangle^f$ becomes equal to sum of the last three terms. Hence following [13], additional appeared terms in Equation 43 can be modeled as follows:

$$R^{k}_{Product} - \frac{\partial}{\partial x_i}\left[\left\langle U_i'' k''\right\rangle^{f}\right] + \frac{1}{\Delta V_f}\int_{A_w} n_i\left[\left(\nu + \frac{\nu_t}{\sigma_k}\right)\frac{\partial k}{\partial x_i}\right] dA = \varepsilon_\infty \quad (44)$$

The asymptotic value of macroscopic dissipation rate of turbulent kinetic energy in homogenous porous media under steady state fully developed flow is ε_∞ and should disappear on the limiting case of clear fluid flow ($\varphi \to 1$). Also, note that the integral term of (44) due to the no-slip boundary condition on fluctuating velocities is always negative, therefore the transport equation of $\langle k\rangle^f$ becomes:

$$\frac{\partial\langle k\rangle^f}{\partial t} + \frac{\partial}{\partial x_i}\left(\left\langle U_i\right\rangle^f\langle k\rangle^f\right) = \frac{\partial}{\partial x_i}\left[\left(\nu + \frac{\nu_t}{\sigma_k}\right)\frac{\partial\langle k\rangle^f}{\partial x_i}\right] + 2\nu_t\left\langle S_{ij}\right\rangle^f\left\langle S_{ij}\right\rangle^f - \langle\varepsilon\rangle^f + \varepsilon_\infty \quad (45)$$

In a similar manner, transport equation for $\langle\varepsilon\rangle^f$ is achieved by applying the volume average operator over the Equation 29, therefore by neglecting the zero remainder integrals we get:

$$\frac{\partial\langle\varepsilon\rangle^f}{\partial t} + \frac{\partial}{\partial x_i}\left(\left\langle U_i\right\rangle^f\langle\varepsilon\rangle^f\right) = \frac{\partial}{\partial x_i}\left[\left(\nu + \frac{\nu_t}{\sigma_k}\right)\frac{\partial\langle\varepsilon\rangle^f}{\partial x_i}\right] - \left[2\nu_t C_1\left\langle S_{ij}\right\rangle^f\left\langle S_{ij}\right\rangle^f + C_2\langle\varepsilon\rangle^f\right]\frac{\langle\varepsilon\rangle^f}{\langle k\rangle^f} - \frac{\partial}{\partial x_i}\left[\left\langle U_i''\varepsilon''\right\rangle^f\right] + \frac{1}{\Delta V_f}\int_{A_w} n_i\left[\left(\nu + \frac{\nu_t}{\sigma_\varepsilon}\right)\frac{\partial\varepsilon}{\partial x_i}\right]dA + R^{\varepsilon}_{Product} \quad (46)$$

Following [13] the additional terms of Equation 46 are modeled as:

$$R^{\varepsilon}_{Product} - \frac{\partial}{\partial x_i}\left[\left\langle U_i''\varepsilon''\right\rangle^f\right] + \frac{1}{\Delta V_f}\int_{A_w} n_i\left[\left(\nu + \frac{\nu_t}{\sigma_k}\right)\frac{\partial\varepsilon}{\partial x_i}\right] dA = C_2\frac{\varepsilon_\infty^2}{k_\infty} \quad (47)$$

k_∞ is the asymptotic value of macroscopic turbulent kinetic energy in homogenous porous media under steady state fully developed flow and should vanish on the limiting case of a clear fluid flow ($\varphi \to 1$), therefore transport equation of macroscopic dissipation rate of turbulent kinetic energy $\langle\varepsilon\rangle^f$ is derived as:

$$\frac{\partial\langle\varepsilon\rangle^f}{\partial t} + \frac{\partial}{\partial x_i}\left(\left\langle U_i\right\rangle^f\langle\varepsilon\rangle^f\right) = \frac{\partial}{\partial x_i}\left[\left(\nu + \frac{\nu_t}{\sigma_k}\right)\frac{\partial\langle\varepsilon\rangle^f}{\partial x_i}\right] - \left[2\nu_t C_1\left\langle S_{ij}\right\rangle^f\left\langle S_{ij}\right\rangle^f + C_2\langle\varepsilon\rangle^f\right]\frac{\langle\varepsilon\rangle^f}{\langle k\rangle^f} + C_2\frac{\varepsilon_\infty^2}{k_\infty} \quad (48)$$

Functional form of k_∞, ε_∞ will be evaluated by solution of $\overline{v^2} - f$ model for the case of the flow through a simulated porous media and will be represented in the sequel.

5. MICROSCOPIC $\overline{v^2} - f$ MODEL CALCULATION AND VALIDATION

Figure 2 depicts a periodic array of square cylinders as a simulated porous media. Only one structural unit shown in Figure 3 is considered for microscopic calculations, according to the periodicity of geometry. The results of these calculations evaluate the macroscopic k-ε model constants (k_∞ and ε_∞ see Section 4).

The Reynolds number is based on the particle diameter D ($Re_D = u_D D/\nu$) and $u_D = \varphi\langle U\rangle^f$ is Darcian velocity. The porosity of the domain is obtained by $\varphi = 1 - (D/H)^2$. Distance between two particles is denoted by H.

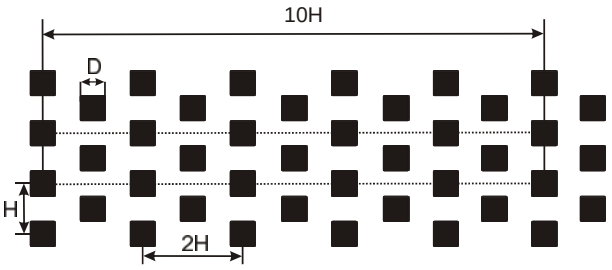

Figure 2. Periodic array of square cylinders.

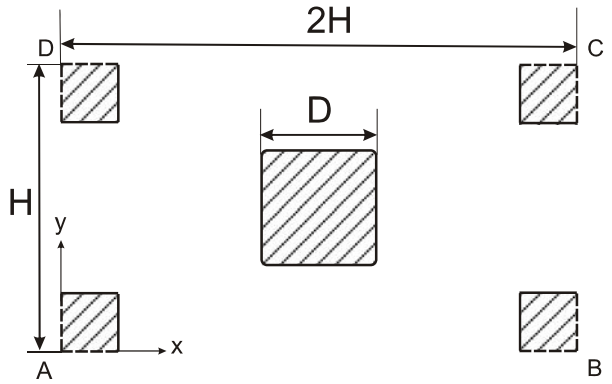

Figure 3. Structural unit chosen for the computational domain.

Boundary conditions for velocity associated to periodicity are as follows:

$$U(x=0.,y)=U(x=2H,y) \tag{49}$$

$$U(x,y=0.)=U(x,y=H) \tag{50}$$

Periodic boundary for pressure is considered according to Kelkar, et al [28].

The periodic boundary conditions for turbulent kinetic energy and its dissipation are as follows:

$$k(x=0.,y)=k(x=2H,y),k(x,y=0.)=k(x,y=H) \tag{51}$$

$$\varepsilon(x=0.,y)=\varepsilon(x=2H,y),\ \varepsilon(x,y=0.)=\varepsilon(x,y=H) \tag{52}$$

Reynolds stress $\overline{v^2}$ and compensated elliptic relaxation $\tilde{f}$ boundary conditions related to periodic geometry can be written as:

$$\begin{aligned}&\overline{v^2}(x=0.,y)=\overline{v^2}(x=2H,y),\\&\overline{v^2}(x,y=0.)=\overline{v^2}(x,y=H)\end{aligned} \tag{53}$$

$$\begin{aligned}&\tilde{f}(x=0.,y)=\tilde{f}(x=2H,y),\\&\tilde{f}(x,y=0.)=\tilde{f}(x,y=H)\end{aligned} \tag{54}$$

Employing Equation 15 no slip boundary conditions are imposed.

The governing equations are discretized using GLS (Galerkin/Least-Squares) finite element method employing equal order bilinear interpolation for velocity and pressure and other variables in conjunction with a pressure stabilizing method (see [29,30] for more details).

Equations 1, 2, 5, 6, 7, 8 are numerically solved inside the domain of Figure 3. The Reynolds number Re_D is varied from 1000 to 84000. Porosities in present calculations are selected out as: φ = 0.3, 0.4, 0.5, 0.64, 0.75, 0.84 and 0.95, respectively, the value of D is varied as 0.83667, 0.7746, 0.7072, 0.6, 0.5, 0.4 and 0.2236 and H is set equal to unity.

For validating the mesh-independency, the flow through the porosity of 0.84 has been solved at Re_D = 3873, 7746, 38730 and 77460 employing 7508, 11948 and 17928 elements. The microscopic turbulent kinetic energy normalized by the square of Darcian velocity k/u_D^2 of three mesh systems for Re_D = 77460 at x/H = 1 are shown in Figure 4. The near wall mesh stretching in these three solutions is similar. There is a good agreement between the solution data of 11948 and 17928 elements, hence mesh systems of order of 12000 seems to be sufficiently accurate and all calculations presented below are obtained for this mesh system. Figure 5 depicts the 11948 elements used for φ = 0.84.

Regarding the numerical convergence, the normalized residuals for all variables were brought down to 10^{-5}. For the Reynolds numbers lower than 5×10^4 the under relaxation coefficient of U and p are 0.8, k and ε are 0.6 and $\overline{v^2}$ and $\tilde{f}$ are 0.5. For Reynolds numbers equal or greater than 5×10^4 the

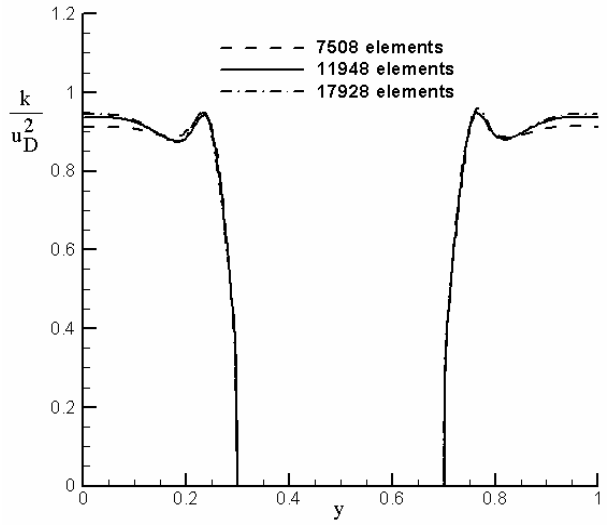

Figure 4. Normalized microscopic turbulent kinetic energy at $Re_D = 40000$, x/H = 1.

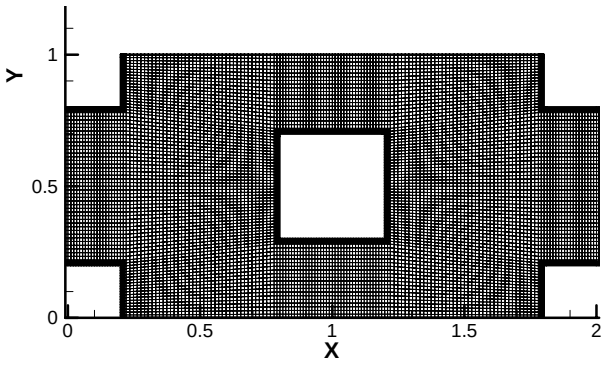

Figure 5. Mesh system of 11948 elements used for φ = 0.84.

under relaxation coefficient of U and P are 0.7, k and ε are 0.4 and $\overline{v^2}$ and $\tilde{f}$ are 0.3, respectively.

Flow streamlines for $Re_D = 40000$ and porosity of 0.84 and pressure contours of this solution are shown in Figures 6 and 7, respectively. Turbulent kinetic energy contours of $Re_D = 40000$ and porosity of 0.84 are depicted in Figure 8.

In the macroscopic turbulence modeling (Equations 42,45), the dependency of intrinsic volume average turbulence characteristics related to porosity are needed. References [13,16] observed that the normalized macroscopic

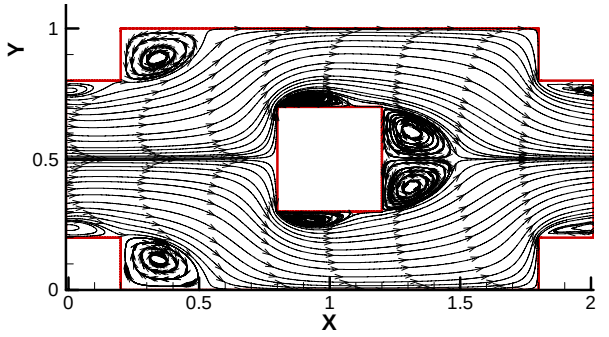

Figure 6. Streamlines, Porosity = 0.84, $Re_D = 40000$.

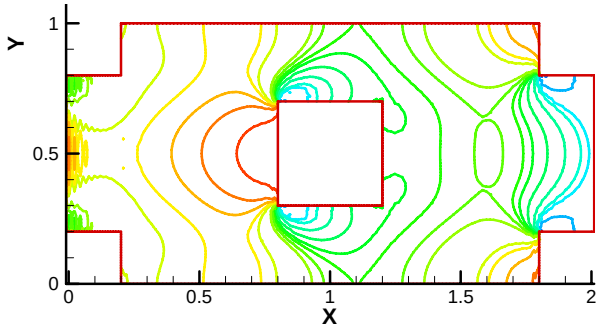

Figure 7. Pressure contours, Porosity = 0.84, $Re_D = 40000$.

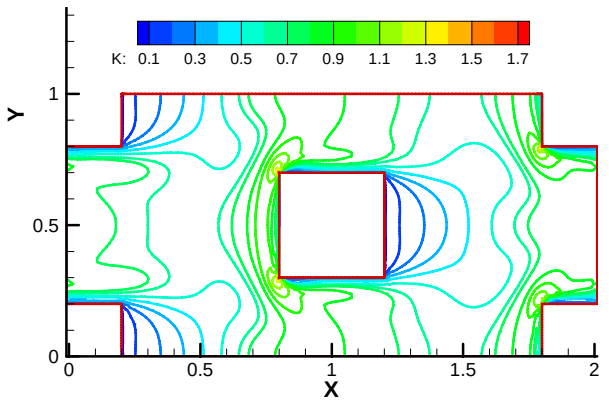

Figure 8. Normalized turbulent kinetic energy contours, Porosity = 0.84, $Re_D = 40000$.

turbulent characteristics remain almost constant at large Reynolds numbers at steady state condition. In the present work this dependency is verified. For example the macroscopic turbulent kinetic

energy and its dissipation rate versus Reynolds number for porosity of 0.64 are depicted in Figures 9 and 10. We can conclude from these figures that the remainders (modeled) terms depend only on porosity.

The turbulent kinetic energy field is converted into macroscopic turbulent kinetic energy using Equation 17 for all selected porosities. Figure 11 depicts the normalized macroscopic turbulent kinetic energies of all selected porosities versus $(1-\varphi)/\varphi^{0.5}$. These data are extracted form the microscopic solution of $\overline{v^2}-f$ model. The results of present study are compared with the result of LES [16] and low Reynolds k-ε solution of [13]. The rate of $\overline{v^2}-f$ model data is smaller than the LES and low Reynolds k-ε model data. At lower porosities the normalized macroscopic turbulent kinetic energy of [16,13] is larger than the $\overline{v^2}-f$ predictions. It is known, that the turbulent kinetic energy predicted by k-ε model is overestimated in the stagnation or impingement region. The difference between k-ε and $\overline{v^2}-f$ model data at lower porosities may be attributed to this reason. The discrepancy between $\overline{v^2}-f$ and LES data can also be attributed to the use of renormalized group (RNG) subgrid scale model in LES [16] leading to overestimation turbulent kinetic energy near stagnation or impingement regions.

Macroscopic turbulent kinetic energies for all selected porosities calculated with $\overline{v^2}-f$ model represent the following correlation:

$$\langle k\rangle^f / u_D^2 = k_\infty / u_D^2 = 3.7(1-\varphi)/\varphi^{0.5} - 2.38\left[(1-\varphi)/\varphi^{0.5}\right]^2 + 0.66\left[(1-\varphi)/\varphi^{0.5}\right]^3 \quad (55)$$

The normalized macroscopic dissipation rates of turbulent kinetic energy for selected porosities in present study are shown in the Figure 12. The present data are compared with the data of Nakayama and Kuwahara [13]. Good agreement is observed. The normalized macroscopic dissipation rates of turbulent kinetic energy data $\langle\varepsilon\rangle^f H/u_D^3$ versus $(1-\varphi)/\varphi^{0.5}$ of Figure 12 represent the following correlation:

$$\langle\varepsilon\rangle^f H/u_D^3 = \varepsilon_\infty H/u_D^3 = 8.73(1-\varphi)/\varphi^{0.5} + 2.1\left[(1-\varphi)/\varphi^{0.5}\right]^2 + 22.6\left[(1-\varphi)/\varphi^{0.5}\right]^3 \quad (56)$$

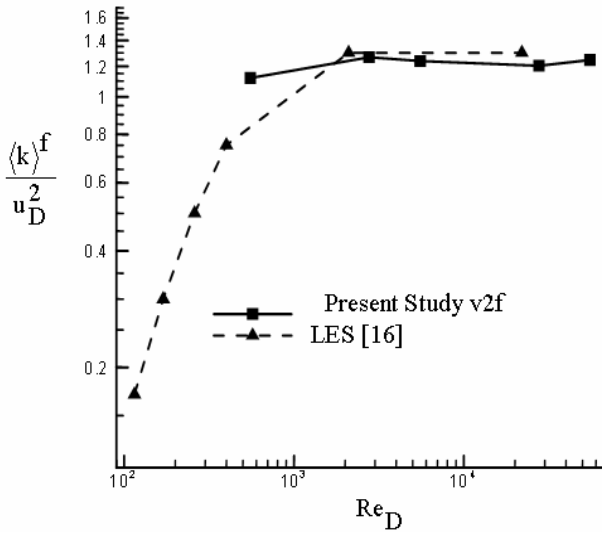

Figure 9. Normalized macroscopic turbulent kinetic energy versus reynolds number, Porosity = 0.64.

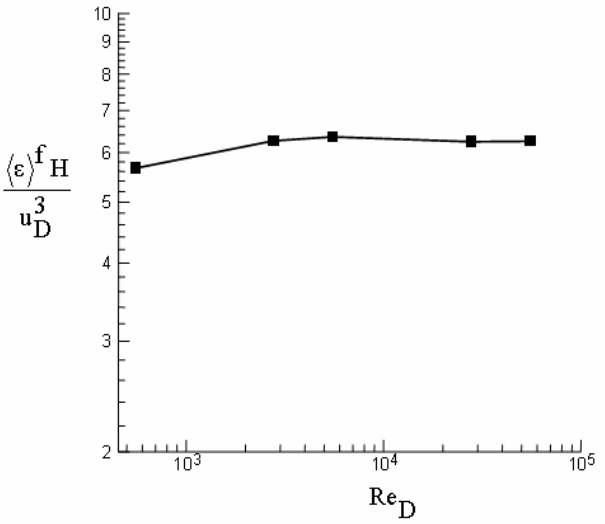

Figure 10. Normalized macroscopic dissipation rate of turbulent kinetic energy versus reynolds number, Porosity = 0.64.

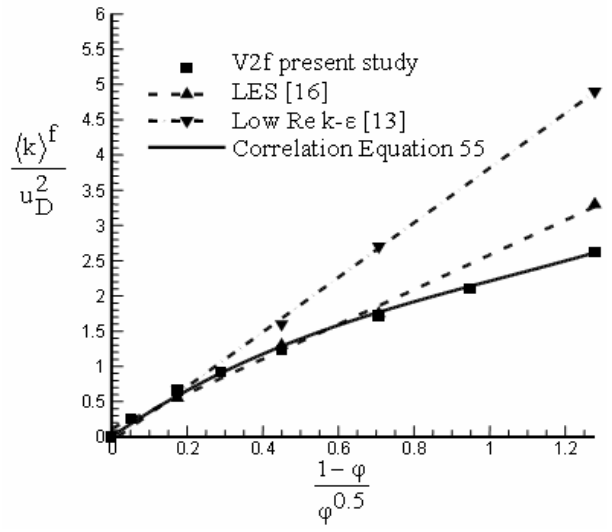

Figure 11. Normalized turbulent kinetic energy versus $\frac{1-\varphi}{\varphi^{0.5}}$.

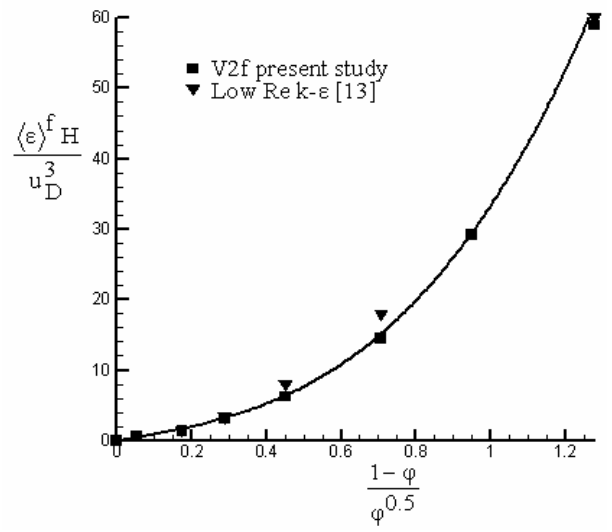

Figure 12. Dissipation of turbulent kinetic energy versus $\frac{1-\varphi}{\varphi^{0.5}}$.

These correlations are employed in modeling the remainder terms of macroscopic k-ε model (see Equations 45,48).

The popular and well-known equation for estimating the pressure drop through porous media is Forchheimer equation. Ergun's empirical equation accounting for the Forchheimer drag in packed beds of particle diameter D is given as [16]:

$$-\frac{d\langle p\rangle^f}{dx}\left[\frac{D}{\rho u_D^2}\right]=\frac{150(1-\varphi)^2}{\varphi}\left(\frac{\nu}{u_D D}\right)+1.75\frac{1-\varphi}{\varphi^3} \quad (57)$$

The first term on the right hand side of Equation 57 could be ignored at high Reynolds number, Following Kuwahara, et al [16], therefore Ergun's equation can be rewritten as follows:

$$-\frac{d\langle p\rangle^f}{dx}\left[\frac{D}{\rho u_D^2}\right]\cong 1.75\frac{1-\varphi}{\varphi^3} \qquad Re_D>3000 \qquad (58)$$

Figure 13 depicts the dimensionless pressure gradient $-d\langle p\rangle^f / dx\left[D/\rho u_D^2\right]$ for selected porosities of this work. Pressure drags predicated by LES [16] are compared with results of $\overline{v^2}-f$ in Figure 13. The line drawn in Figure 13 represents the Ergun's equation. Pressure gradient results of present study are in good agreement with Ergun's equation.

6. VALIDATING THE "$\overline{v^2}-f$ BASED" MACROSCOPIC k-ε TURBULENCE MODEL

In order to evaluate the macroscopic "$\overline{v^2}-f$ based" k-ε model, we solve a steady unidirectional highly turbulent flow entering into a semi-finite periodic array of square rods, with macroscopic points of view. The case study of this section is five times longer than the case study in Section 5. The inlet conditions are uniform and developed outflow boundary conditions are considered.

From the microscopic point of view, we solve a steady unidirectional highly turbulent flow entering into a semi-finite periodic array of square rods (Figure 2), with employing $\overline{v^2}-f$ model. Microscopic governing Equations 1, 2, 5, 6, 7 and 8 are solved over five cells solution (dotted area in

Figure 2). Periodic boundary conditions are imposed only to upper and lower boundaries. The Reynolds number is $Re_D = 7.07 \times 10^4$ and porosity $\varphi = 0.75$. Inlet values for velocity profile are fixed equal to unity and inlet pressure is considered as a finite value. The inlet values for turbulent kinetic energy and its dissipation are assumed as:

$$\left.\frac{\langle k\rangle^f}{u_D^2}\right|_{x=0} = 10. \quad (59)$$

$$\left.\frac{\langle \varepsilon\rangle^f H}{u_D^3}\right|_{x=0} = 30. \quad (60)$$

These boundary conditions are in accordance with the inlet boundary conditions of [13]. The normal Reynolds stress $\overline{v^2}$ inlet boundary condition is as follow:

$$\left.\frac{\left\langle \overline{v^2}\right\rangle^f}{u_D^2}\right|_{x=0} = \frac{2}{3}\times\left.\frac{\langle k\rangle^f}{u_D^2}\right|_{x=0} = 6.667 \quad (61)$$

Compensated elliptic relaxation inlet boundary condition is as follow:

$$\left.\frac{\langle \tilde{f}\rangle^f H}{u_D}\right|_{x=0} = 10. \quad (62)$$

The inlet boundary condition for compensated elliptic relaxation is computed from Equation 16 using inlet values of $\langle k\rangle^f$, $\langle \varepsilon\rangle^f$ and $\left\langle \overline{v^2}\right\rangle^f$. At the outlet, fully developed conditions are imposed for all variables.

Figure 14 shows flow streamlines of large scale solution of microscopic $\overline{v^2}-f$ model at $Re_D = 7.07 \times 10^4$ for porosity $\varphi = 0.75$. Turbulent kinetic energy contours of this solution are depicted in Figure 15.

After obtaining the flow solution with employing the $\overline{v^2}-f$ model, microscopic results of turbulence quantities are integrated over the domain in order to study the developments of macroscopic turbulent kinetic energy and its dissipation rate. The agreement between the one-cell solution data and fifth cell of large scale solution indicates that the flow is fully developed in the five cells long domain (see Figure 16).

In the modeling context, we solve the macroscopic continuity and momentum Equations

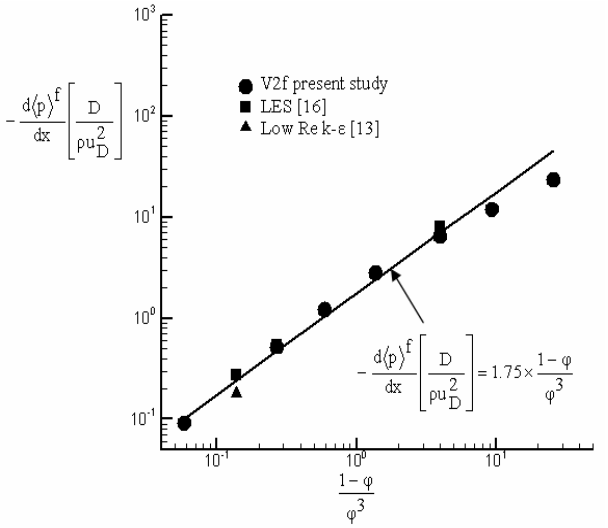

Figure 13. Dimensionless macroscopic pressure gradient versus $\frac{1-\varphi}{\varphi^3}$.

Figure 14. Large scale microscopic solution streamlines, $Re_D = 7.07 \times 10^4$.

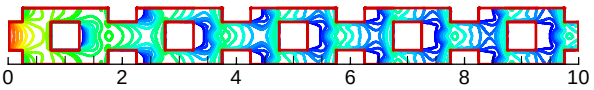

Figure 15. Large scale microscopic solution, turbulent kinetic energy contours, $Re_D = 7.07 \times 10^4$.

24, 25 with employing the "$\overline{v^2}-f$ based" macroscopic k-ε model Equations 45, 48 in conjunction with macroscopic correlations Equations 55 and 56, over the dotted area of Figure 2, consistent with a macroscopic point of view.

For validating the accuracy of "$\overline{v^2}-f$ based" macroscopic k-ε model, data of this macroscopic solution are compared with the averaged solution data of microscopic solution of $\overline{v^2}-f$ model. Figure 16 depicts macroscopic turbulent kinetic energy's field predicted by microscopic $\overline{v^2}-f$ model and "$\overline{v^2}-f$ based" macroscopic k-ε model. Figure 16 indicates that macroscopic turbulent kinetic energies of all solutions of present work are in a good agreement which low Reynolds k-ε data of [13]. As we expected, the value of turbulent kinetic energy computed from "$\overline{v^2}-f$ based" k-ε model and $\overline{v^2}-f$ model are lower than k-ε model of [13].

Figure 17 shows the macroscopic field of dissipation rate of turbulent kinetic energy obtained from calculation of microscopic $\overline{v^2}-f$ model and "$\overline{v^2}-f$ based" macroscopic k-ε model. These results are also compared with the solution of low Reynolds number k-ε model of [13]. Good matching is observed between macroscopic data of "$\overline{v^2}-f$ based" model, macroscopic values averaged from the microscopic $\overline{v^2}-f$ model and macroscopic data of [13].

For a more rigorous validation of the "$\overline{v^2}-f$ based" macroscopic k-ε model, the macroscopic model is solved for porosities 0.3, 0.4, 0.5, 0.64, 0.75, 0.84 and 0.95. Note that for the case of fully developed steady state flow, the values predicated by "$\overline{v^2}-f$ based" macroscopic k-ε model have to be consistent with correlations given by Equations 55 and 56 for the same porosity. The predicted values of "$\overline{v^2}-f$ based" macroscopic k-ε and values of correlations extracted from microscopic

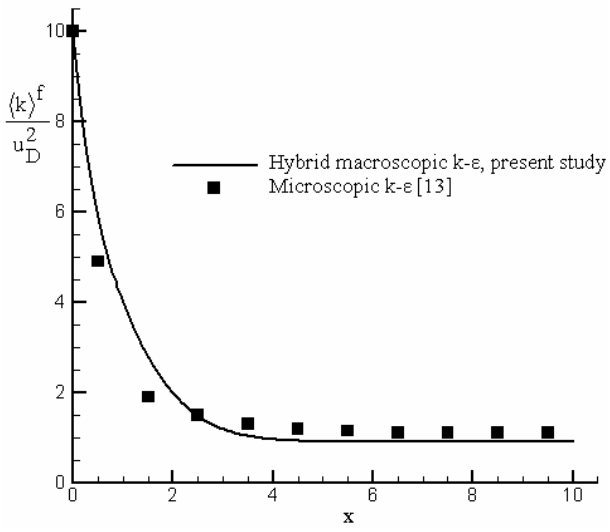

Figure 16. Development of turbulence kinetic energy through porous media for porosity = 0.75, $Re_D = 7.07 \times 10^4$.

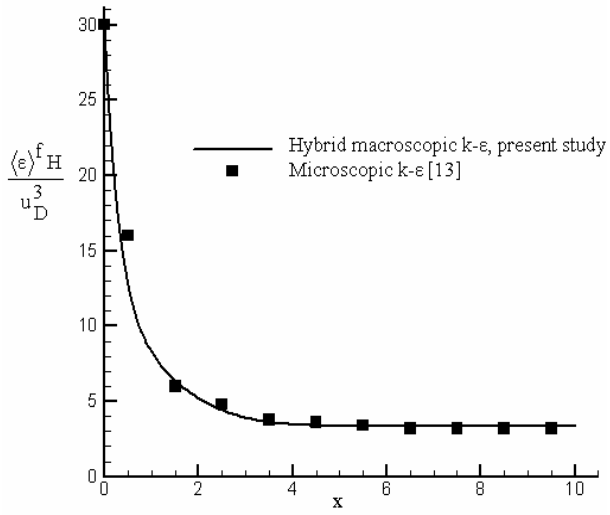

Figure 17. Development of dissipation rate of turbulence kinetic energy through porous media for porosity = 0.75, $Re_D = 7.07 \times 10^4$.

$\overline{v^2}-f$ model solutions (see Section 5) are compared in Tables 1 and 2. The relative errors between two values are shown in these tables. The matching between two data reveals the good performance of the proposed correlations and model.

TABLE 1. Values of $\langle k\rangle^f / u_D^2$ Predicted from Equation 57, from Microscopic Model, and from Macrscopic Model.

Porosity	$\langle k\rangle^f / u_D^2$ from "$\overline{v^2}-f$ Based" Macroscopic k-ε Model	$\langle k\rangle^f / u_D^2$ from Microscopic $\overline{v^2}-f$ Model	$\langle k\rangle^f / u_D^2$ from Equation 57	Relative Error of 1st Column with Respect to Microscopic Data %
0.3	2.155	2.13	2.219	1.2
0.4	1.922	1.97	1.932	2.4
0.5	1.67	1.66	1.660	0.6
0.64	1.26	1.246	1.243	1.1
0.75	0.902	0.8847	0.886	2.0
0.84	0.588	0.6783	0.577	13.3
0.95	0.188	0.260	0.184	27.7

TABLE 2. Values of $\langle \varepsilon\rangle^f H / u_D^3$ Predicted from Equation 58, from Microscopic Model, and from Macrscopic Model.

Porosity	$\langle \varepsilon\rangle^f H / u_D^3$ from "$\overline{v^2}-f$ Based" Macroscopic k-ε Model	$\langle \varepsilon\rangle^f H / u_D^3$ form Microscopic $\overline{v^2}-f$ Model	$\langle \varepsilon\rangle^f H / u_D^3$ from Equation 58	Relative Error of 1st Column with Respect to Microscopic Data %
0.3	59.54	58.92	61.76	1.1
0.4	29.25	29.14	29.46	0.4
0.5	15.36	14.54	15.21	5.6
0.64	6.55	6.253	6.41	4.7
0.75	3.327	3.183	3.24	4.5
0.84	1.76	1.617	1.71	8.8
0.95	0.472	0.4563	0.46	3.4

6.1. Real Problem In this section we solve a real problem defined in the experimental research of [31], regarding pressure drop in a packed bed. The cross sectional scheme of the main apparatus used in this experiment is depicted in Figure 18. The size of rectangular container is 0.304 m by 0.760 m by 0.760 m and it is connected with a blower by a tube equipped with a gate valve and an orifice plate in order to fix air flow rate. 3200 table tennis balls glued together in a simple cubic array of size 8 by 20 by 20 spheres are filled the container. The uniform packing core was formed by cells [31].

The Reynolds number is $Re_D = 1800$ and porosity is $\varphi = 0.476$. The friction factor f_f of porous media is defined as:

$$f_f = -\frac{d\langle p\rangle^f}{dx}\left[\frac{D}{\rho u_D^2}\right] \quad (63)$$

In this problem, macroscopic "$\overline{v^2}-f$ based" k-ε model of present study and macroscopic k-ε model of Nakayama, et al [13] are solved for the same porosity and Reynolds number. Ergun's friction factor was computed from Equation 63. Tobis [31] numerically solved flow through this packed bed with employing k-ε model, using a microscopic point of view and friction factor was computed from the result of numerical solution. All the computed results in the present work are compared with the numerical and experimental results of [31] in Table 3. There is a good agreement between macroscopic $\overline{v^2}-f$ model and Experimental data of [31]. The over-prediction of k-ε result is consistent with inherent shortcomings of this model.

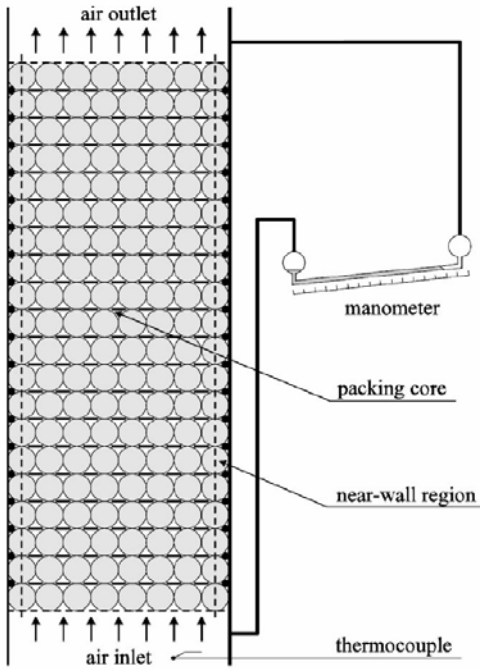

Figure 18. Schematic view of experimental equipment [31].

TABLE 3. Values of Friction Factor Predicted from Macroscopic "$\overline{v^2}-f$ Based "k-ε Model, Experimental Data [28], Ergun Correlation [16] and Macroscopic k-ε Model of Nakayama, et al [13].

Mac. "$\overline{v^2}-f$ Based" k-ε Model	Mac. k-ε Model [13]	k-ε Model [31]	Experiment [31]	Ergun [16]
6.03	6.66	5.8	6(±15%)	8.4(±50%)

7. CONCLUSION

A reliable model is needed to simulate turbulent flow in porous media for engineers and researchers involved in industry and research oriented projects. The only plausible engineering method for the foreseen future is turbulence modeling, in conjunction with volume averaging technique to circumvent the necessity to resolve all flow features and to simulate the turbulence structures in the pores. Among different models introduced in the context of RANS, the $\overline{v^2}-f$ model which is a more refined, and have been successful for solving recirculating non-isotropic clear flows seems to be a good candidate, and a tentative analysis of its performance for porous media could render useful results. However, it has to be mentioned that LES also may lead to realistic results in near future and this work is not attempting to compare the relative pros and cons of LES and RANS models. We believe that the prediction of $\overline{v^2}-f$ model in porous media is superior to k-ε model and its performance may be interesting for engineering communities and commercial code developers in the field of porous media.

In this work, the continuity and momentum equations for incompressible flow are solved in conjunction with $\overline{v^2}-f$ model. Macroscopic k-ε transport equations derived for porous media employing a volume averaging technique. The additional terms appear in the macroscopic k-ε model due to averaging process were modeled by solutions of microscopic $\overline{v^2}-f$ model. The numerical computations conducted for a wide range of porosities are encouraging for the geometry/morphology examined in this paper. The modeling results seem reliable when compared to respected microscopic fields calculated using conventional microscopic point of view. Friction factor of flow through packed beds predicted from present "$\overline{v^2}-f$ based" macroscopic k-ε model which was compared with the available experimental data and good agreement was observed. We believe that the proposed model in the present study reconciles the relative robustness of k-ε model with the superior accuracy of $\overline{v^2}-f$ model. However, further work should be conducted for more complicated and complex situations to rigorously criticize the model proposed in this work.

8. NOMENCLATURE

A_w	Interface area between solid and fluid phase in porous media
$C_L, C_T, C_\mu, C_\eta, C_1, C_2, C_{\varepsilon 1}, C_{\varepsilon 2}$:	Turbulence model constants
D	Particle diameter
f	Elliptic relaxation function
$\tilde{f}$	Compensated elliptic relaxation function
f_f	Friction Factor
H	Distance between two particles
k	Turbulent kinetic energy
$\langle k \rangle^f$	Intrinsic volume average of turbulent kinetic energy
L	Turbulent length scale
P	Pressure
P_k	Production of turbulent kinetic energy
$R^k_{Product}$	Remainder term of production of turbulent kinetic energy
$R^\varepsilon_{Product}$	Remainder term of production of dissipation of turbulent kinetic energy
Re_D	Reynolds number based on *D*
Re_P	Reynolds number based on particle dimension
S_{ij}	Strain rate tensor
t	Time
T	Turbulent time scale
U	Time averaged velocity vector
u	Time fluctuation velocity vector
u_D	Darcian velocity
V	Total volume of porous media
V_f	Volume of fluid in porous media
$\overline{v^2}$	Normal to the wall component of Reynolds stress
x_i	Coordinate components

8.1. Greek Letters

δ_{ij}	Kronecker delta
ε	Dissipation rate of turbulent kinetic energy
$\langle\varepsilon\rangle^f$	Intrinsic volume average of dissipation rate of turbulent kinetic energy
φ	Porosity
ν	Kinematics viscosity
ν_t	Turbulent kinematics viscosity
ρ	Density
$\sigma_k, \sigma_\varepsilon$	Turbulence model constants

9. REFERENCES

1. Dybbs, A. and Edwards, R. V., "A new look at Porous Media Fluid Mechanism-Darcy to Turbulent", In Fundamentals of Transport Phenomena in Porous Media (Book), Editors: Bear, J. and Corapcioglu, V., Martinus Nijhoff, The Netherlands, (1984), 199-254.
2. Missirlis, D., Yakinthos, K., Palikaras, A., Katheder, K. and Goulas, A., "Experimental and Numerical Investigation of the Flow Field Through a Heat Exchanger for Aero-Engine Applications", ***Int. J. of Heat and Fluid Flow***, Vol. 26, (2005), 440-458.
3. Yang, Y. T. and Hwang, C. Z., "Calculation of Turbulent flow and Heat Transfer in a Porous-Baffled Channel", ***Int. J. of Heat and Mass Transfer***, Vol. 46, (2003), 771-780.
4. Garcia, N., Lara, J. L. and Losada, I. J., "2-D Numerical Analysis of Near-Field flow at Low-Crested Permeable breakwaters", ***Coastal Engineering***, Vol. 51, (2004), 991-1020.
5. Karim, M. F. and Tingsanchalil T., "A Coupled Numerical Model for Simulation of Wave Breaking and Hydraulic Performances of a Composite Seawall, ***Ocean Engineering***, Vol. 33, (2006), 773-787.
6. Prescott, P. J. and Incropera, F. P., "The Effect of Turbulence on Solidification of a Binary Metal Alloy with Electromagnetic Stirring", ***ASME J. Heat Transfer***, Vol. 117, (1995), 716-724.
7. Chandesris, M., Serre, G. and Sagaut, P., "A Macroscopic Turbulence Model for flow in Porous Media Suited for Channel Pipe and Rod Bundle flows", ***Int. J. Heat Mass Transfer***, Vol. 49, (2006), 2739-2750.
8. Masuoka, T. and Takatsu, Y., "Turbulence Model for flow Through Porous Media", ***Int. J. Heat Mass Transfer***, Vol. 39, (1996), 2803-2809.
9. Alvarez, G., Bournet, P. E. and Flick, D., "Two Dimensional Simulations of Turbulent flow and Transfer through Stacked Spheres", ***Int. J. Heat Mass Transfer***, Vol. 46, (2003), 2459-2469.
10. Antohe, B. V. and Lage, J. L., "A General Two-Equation Macroscopic Turbulence Model for Incompressible flow in Porous Media", ***Int. J. Heat Mass Transfer***, Vol. 40, (1997), 3013-3024.
11. Getachew, D., Minkowycz, W. J. and Lage, J. L., "A Modified form of the k-ε Model for Turbulent flows of an Incompressible Fluid in Porous Media", ***Int. J. Heat Mass Transfer***, Vol. 43, (2000), 2909-2915.
12. Kuwahara, F., Kameyama, Y., Yamashita, S. and Nakayama, A., "Numerical Modeling of Turbulent flow in Porous Media using a Spatially Periodic Array", ***J. Porous Media***, Vol. 1, (1998), 47-55.
13. Nakayama, A. and Kuwahara, F., "A Macroscopic Turbulence Model for flow in a Porous Medium", ***ASME J. Fluids Eng***., Vol. 121, (1999), 427-433.
14. Pedras, H. J. and de Lemos, M. J. S., "Macroscopic Turbulence Modeling for Incompressible flow through Undeformable Porous Media", ***Int. J. Heat Mass Transfer***, Vol. 44, (2001), 1081-1093.
15. de Lemos, M. J. S., "Turbulence in Porous Media Modeling and Applications", Elsevier, Amsterdam, The Netherlands, (2006).
16. Kuwahara, F., Yamane, T. and Nakayama, A., "Large Eddy Simulation of Turbulent flow in Porous Media", ***Int. Com. in Heat and Mass Transfer***, Vol. 33, (2006), 411-418.
17. Durbin, P. A., "Near-Wall Turbulence Closure Modeling Without Damping Functions", **Theoretical *and Computational Fluid Dynamics***, (1991), 1-13.
18. Durbin, P. A., "On the k-ε Stagnation Point Anomaly", ***Int. J. of Heat and Fluid Flow***, Vol. 17, (, 1995), 89-90.
19. Durbin, P., "Separated flow Computations with the $k-\varepsilon-\overline{v^2}$ Model", ***AIAA Journal***, Vol. 33, (1995), 659-664.
20. Behnia, M., Parneix, S. and Durbin, P. A., "Prediction of Heat Transfer in an Axisymmetric Turbulent Jet Impinging on a Flat Plate", ***Int. J. Heat Mass Transfer***, Vol. 41, (1998), 1845-1855.
21. Lien, F. S. and Kalitzin, G., "Computations of Transonic flow with the $\overline{v^2}-f$ Turbulence Model", ***Int. J. of Heat and Fluid Flow***, Vol. 22, (2001), 53-61.
22. Sveningsson, A. and Davidson, L., "Assessment of Realizability Constraints in $\overline{v^2}-f$ Turbulence Models", ***Int. J. of Heat and Fluid Flow***, Vol. 25, (2004), 785-794.
23. Davidson, L., Nielsen, P. V. and Sveningsson, A., "Modification of the $\overline{v^2}-f$ Model for Computing the flow in a 3D Wall Jet", ***In 4th Int. Symp. on Turbulence Heat and Mass Transfer***, Editors: Hanjalic, K., Nagamo, Y. and Tummer, H., Antalya, Turkey, (2003), 577-584.
24. Whitaker, S., "Advances in Theory of Fluid Motion in Porous Media", ***Ind. Eng. Chem***., Vol. 61, (1969), 14-28.
25. Gray, W. G. and Lee, P. C. Y., "On the Theorems for Local Volume Averaging of Multiphase System", ***Int. J.***

Multiphase Flow, Vol. 3, (1977), 333-340.
26. Vafai, K., "Convection flow and Heat Transfer in Variable Porous Media", ***J. Fluid Mech***., Vol. 147, (1984), 233-259.
27. Launder, B. E. and Spalding, D. B., "Mathematical Model of Turbulence", Academic Press, London and New York, (1972).
28. Kelkar, K. M. and Patankar, S. V., "Numerical Prediction of flow and Heat Transfer in a Parallel Plate Channel with Staggered Fins", ***J. of Heat Transfer***, Vol. 109, (1987), 25-29.
29. Hannani, S. K., Stanislas, M. and Dupont, P., "Incompressible Navier-Stokes Computations with SUPG and GLS Formulations-A Comparison Study", ***Computer Methods in Applied Mechanics and Engineering***, Vol. 124, (1995), 153-170.
30. Hannani, S. K. and Stanislas, M., "Incompressible Turbulent flow Simulation using a Galerkin/Least-Squares Formulation and a Low Reynolds k-ε Model, Comput", ***Methods Appl. Mech. Engineering***, Vol. 181, (2000), 107-116.
31. Tobis, J., "Influence of Bed Geometry on Its Frictional Resistance under Turbulent flow Conditions", ***Chemical Engineering Science***, Vol. 55, (2000), 5359-5366.